



Research papers

Modeling colloid transport in fractures with spatially variable aperture and surface attachment

Scott C. James^{a,*}, Lichun Wang^b, Constantinos V. Chrysikopoulos^c^a Departments of Geosciences and Mechanical Engineering, Baylor University, Waco, TX, United States^b Institute of Surface-Earth System Science, Tianjin University, Tianjin, China^c School of Environmental Engineering, Technical University of Crete, Greece

ARTICLE INFO

This manuscript was handled by Peter K. Kitanidis, Editor-in-Chief, with the assistance of Martin Thullner, Associate Editor

Keywords:

Colloid transport
Particle tracking
Wall effects on diffusion
DLVO attachment

ABSTRACT

A particle-tracking algorithm was developed to simulate colloid transport subject to wall effects on diffusion as well as colloid surface attachment as described by DLVO kinetics. The effects of spatially variable fracture surface potential, which contributed to spatially variable attachment strength affecting colloid transport, were investigated. The fracture surface potential was assumed to be either positively, neutrally (zero), or negatively correlated with the lognormally distributed local fracture aperture, described with a mean, variance, and isotropic correlation length. The results from several model simulations indicated that wall effects were negligible for the synthetic fractures studied here. When fracture surface potential was negatively correlated with local aperture, colloids were preferentially transported through the fracture, because they tended to enter high-flow, large-aperture regions where they underwent less attachment (have the largest first moment measured upon exit of the first colloid from the fracture). The variance (second moment) increased for flowing colloids when comparing negatively to zero and then positively correlated surface potentials to fracture apertures, because spreading notably increased when suspended colloids were temporarily attached onto fracture surfaces. For colloids attached onto fracture surfaces, both first and second moments decreased from negatively, to neutrally (zero), to positively correlated surface potentials to apertures. This is an intuitive result, consistent with fewer colloids attaching along the larger aperture preferential flow paths.

1. Introduction

Studying the physicochemical behavior of colloids in variable-aperture fractures is an important aspect in characterizing their transport therein (Berkowitz, 2002; Zhang et al., 2012). The spatial moments of these colloids are integral to understanding co-transport of hazardous materials in subsurface environments. For example, radioactive wastes are stored in fractured-rock systems (Bossart et al., 2001; Kickmaier et al., 2000; McKenna and James, 2007; NRC, 1999; NUMO, 2004). In geologic formations with low matrix permeability, the primary conduit for fluid flow is through fractures (Cardenas et al., 2007). Therefore fractures and the presence of colloids within a saturated fracture system may enhance the transport of low-solubility, sorptive contaminants (James et al., 2005).

Colloids range in size from 10^{-3} to $10 \mu\text{m}$ in diameter and can be fine particles of minerals, biocolloids (viruses, bacteria), and organic macromolecules (Elimelech et al., 1995). Fine particles of minerals are commonly found in groundwater due to well drilling or the

introduction of cementing agents. In fractured media, colloids are typically formed by microerosion of matrix minerals and can be generated by formation crushing associated with tectonic activity (Drever, 1985). Colloids can also move through groundwater systems faster than conservative solutes, due in part to their low diffusivity preventing them from flowing into regions with low velocities (Bales et al., 1989). Because colloids have a large surface-area-to-volume ratio, sorbing contaminants are afforded the opportunity to migrate with these particles (Ouyang et al., 1996). In addition, if the colloid is assumed to travel at the flow speed at its centroid, the physical size of the colloid prohibits it from sampling the slowest moving portions of the velocity profile nearest the wall (Stoll et al., 2017).

To fully understand generalized colloid transport in water-saturated fractures, attachment dynamics and wall effects in a variable-aperture fracture must be considered. Generating multiple fracture realizations facilitates a quantitative understanding of the flow and transport of these particles while assessing uncertainty. In this study, fracture apertures were assigned according to a lognormally distributed and

* Corresponding author.

E-mail address: sc_james@baylor.edu (S.C. James).

spatially correlated random field using statistical measurements from a real fracture (Wang and Cardenas, 2014). Colloid-wall effects were first considered. Then, fracture aperture and fracture surface potential were randomly varied for each fracture realization. Ultimately, colloid transport through variable-aperture fractures subject to attachment was simulated.

2. Model development

2.1. Variable-aperture fracture generation

A fractured, welded rhyolitic tuff ($12 \times 15 \times 4 \text{ cm}^3$) from the Santana Formation in Trans-Pecos, Texas, USA was examined by X-ray computed tomography to measure the aperture at approximately 0.23-mm horizontal resolution (Cardenas et al., 2007). These aperture data were supplied to the Variogram Estimation and Spatial Prediction Plus ERror (VESPER) program, a variogram and kriging modeling software, to estimate the statistical parameters describing aperture variability (Minasny et al., 1999). The modified fracture-aperture data comprising 240,400 rows of x (m), y (m), and b (aperture, m) were input to VESPER to determine the aperture mean (0.46 mm), variance (0.25 mm^2), and isotropic correlation length ($\sim 12 \text{ mm}$) fit with a spherical variogram. These parameters were used to generate 100 realizations of aperture fields for 4-m-long by 2-m-wide, 3D fractures using the code SPRT2D (Gutjahr, 1989), which uses a Fast Fourier Transform method. Grid cells were $1 \times 1 \text{ mm}^2$. Fig. 1 is an example color plot of the 8 million fracture apertures generated with SPRT2D.

2.2. Flow field calculation

Because the ratios of fracture length- and width-to-aperture were so large, a quasi-3D assumption was made meaning that advective flows perpendicular to the fracture were implemented through z coordinate scaling as a colloid transitioned from one model cell with a given fracture aperture to another with a different aperture (James and Chrysikopoulos, 2000). Of course, diffusion in the z direction was always considered. The hydraulic head throughout the fracture was calculated using the modified Local Cubic Law of Wang et al. (2015) by solving the 2-D, steady-state, partial differential equation describing Newtonian fluid flow in a spatially variable fracture (Abdel-Salam and Chrysikopoulos, 1995):

$$\frac{\partial}{\partial x} \left[\hat{b}^3(x, y) \frac{\partial \eta(x, y)}{\partial x} \right] + \frac{\partial}{\partial y} \left[\hat{b}^3(x, y) \frac{\partial \eta(x, y)}{\partial y} \right] = 0, \quad (1)$$

where \hat{b}^3 (m^3) is the modified local aperture cubed, which considers roughness and tortuosity, and η (m) is the piezometric head throughout a fracture. Boundary conditions were assigned as no-flux along the y boundaries and constant heads along the x boundaries driving flow from left to right. Each head field required solution of a $32,000,000 \times 32,000,000$ matrix, which was solved in minutes with a MatLab sparse-matrix solver that required $>35 \text{ GB}$ of memory.

Next, the in-plane average velocity vectors in the x and y directions were calculated for every variable-aperture cell from the steady-state η field as:

$$u_x(x, y) = -\frac{\gamma \hat{b}^2(x, y)}{12\mu} \frac{\partial \eta(x, y)}{\partial x}, \quad (2)$$

$$u_y(x, y) = -\frac{\gamma \hat{b}^2(x, y)}{12\mu} \frac{\partial \eta(x, y)}{\partial y}, \quad (3)$$

where γ (N m^{-3}) is the fluid specific weight and μ (Pa s) is the fluid dynamic viscosity. Velocity profiles were parabolic in the z direction (i.e., normal to the fracture plane) and governed advection through the 3-D rough fractures. The flow field for Fig. 1 subject to 0.025 m of head difference across the x direction is shown in Fig. 2.

2.3. Particle tracking

Particle tracking was used for simulating colloid transport instead of a 2-D finite-element or finite-difference solution. This is because the particle-tracking algorithm is a stochastic solution to the linear partial differential advection–dispersion equation and particles are tracked individually so that each retains its own characteristics including sorption status and effects due to wall proximity (Delay et al., 2005). Hence, the impact of irregular boundaries of the 3-D variable-aperture fracture on colloid transport were well preserved.

Particle tracking has often been used to study transport in porous and fractured media (James and Chrysikopoulos, 1999; James and Chrysikopoulos, 2000; James and Chrysikopoulos, 2004; James and Chrysikopoulos, 2011; James et al., 2005; Kinzelbach, 1988; Reimus and James, 2002; Smith and Schwartz, 1980; Wang and Cardenas, 2015). The general particle-tracking transport equation consists of an

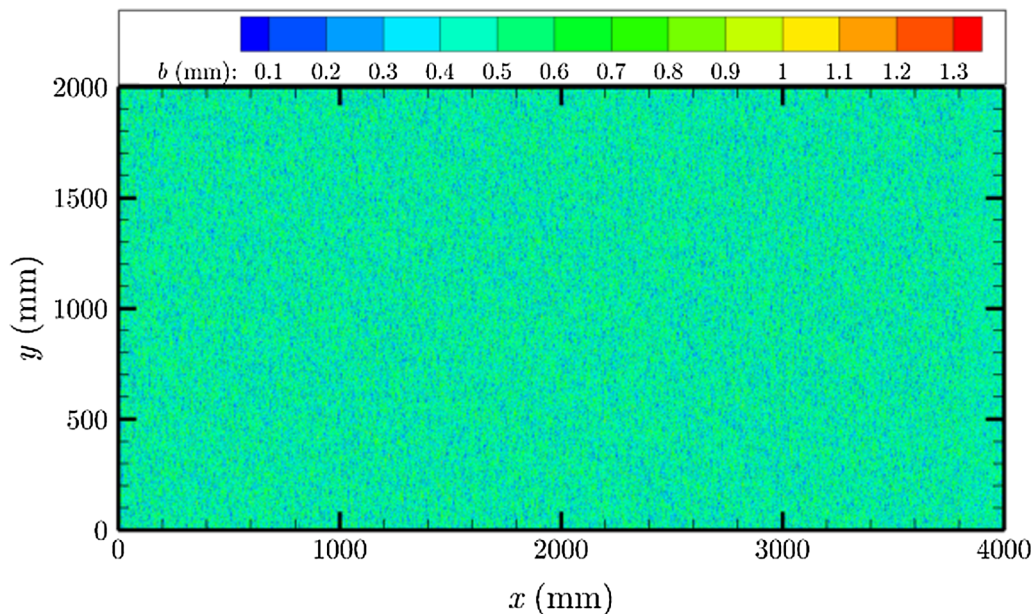


Fig. 1. Color map of one realization of the variable-aperture fractures.

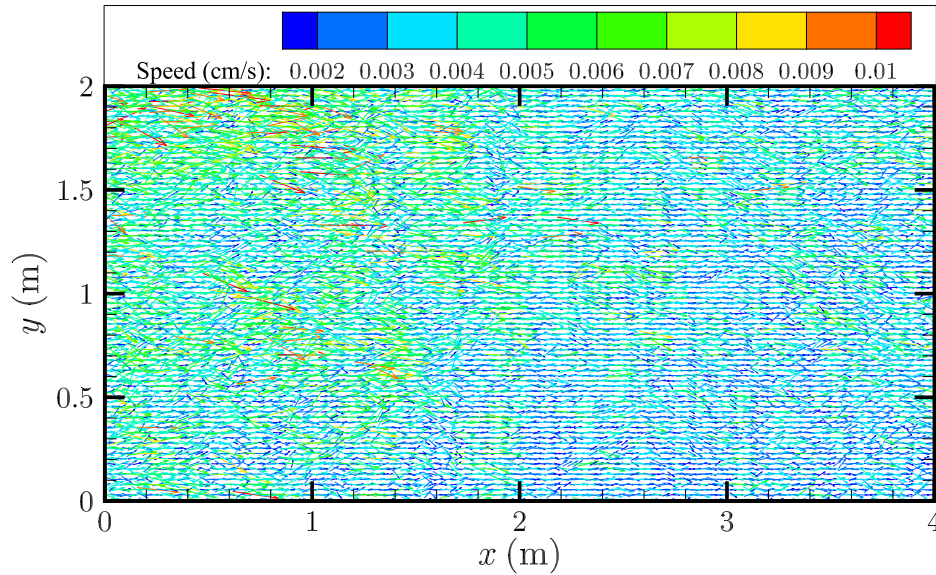


Fig. 2. Velocity field corresponding to the variable-aperture fracture of Fig. 1.

absolute term representing advection and a stochastic term representing random molecular diffusion (Kitanidis, 1994). In vector notation (Tompson and Gelhar, 1990):

$$\mathbf{x}^{m+1} = \mathbf{x}^m + \mathbf{a}(\mathbf{x}^m)\Delta t + \mathbf{B}(\mathbf{x}^m) \cdot \mathbf{n} \sqrt{\Delta t}, \quad (4)$$

where m (–) is the numerical step number, \mathbf{x}^m (m) is the 3-D position vector at time level $m\Delta t$, $\mathbf{a}(\mathbf{x}^m)$ (m s^{-1}) is the forcing vector due to advection, for example, the velocity field evaluated at \mathbf{x}^m , $\mathbf{B}(\mathbf{x}^m)$ ($\text{m s}^{-1/2}$) is a deterministic scaling tensor evaluated at \mathbf{x}^m due to random diffusion, and \mathbf{n} (–) is a vector of three random, independent selections from the standard normal distribution.

2.4. Advection

The forcing vector along the plane of the fracture was due to the Poiseuille velocity profile assumed to exist locally in each fracture-aperture cell plus terms to account for the diffusivity gradients ($\partial D_{\parallel}/\partial x$, $\partial D_{\parallel}/\partial y$, and $\partial D_{\perp}/\partial z$) induced by wall effects (Tompson and Gelhar, 1990):

$$\begin{bmatrix} a_x(x, y, z) \\ a_y(x, y, z) \\ a_z(z) \end{bmatrix} = \begin{bmatrix} \frac{3}{2}u_x(x, y) \left(1 - 4 \left[\frac{z}{b(x, y)} \right]^2 \right) + \frac{\partial D_{\parallel}}{\partial x} \\ \frac{3}{2}u_y(x, y) \left(1 - 4 \left[\frac{z}{b(x, y)} \right]^2 \right) + \frac{\partial D_{\parallel}}{\partial y} \\ \frac{\partial D_{\perp}}{\partial z} \end{bmatrix}, \quad (5)$$

where x , y , and z (m) are the coordinates of the centroid of the colloid, and D_{\perp} (m s^{-2}) and D_{\parallel} (m s^{-2}) are diffusions normal and parallel to the wall, respectively.

2.5. Diffusion

Brownian diffusion of colloid particles must be modified near fracture walls to account for translation and rotation of a sphere in shear flow (Goldman et al., 1967). The specific effects of fracture roughness were not considered with regard to diffusion although aperture variability impacted the flow field. At small separation distances from the wall, both parallel and normal diffusion were modified (decreased) by the hydrodynamic drag force due to wall proximity. Tensor \mathbf{B} in (4) is (Ahlstrom et al., 1977):

$$\mathbf{B} = \begin{bmatrix} \sqrt{2D_{\parallel}} & 0 & 0 \\ 0 & \sqrt{2D_{\parallel}} & 0 \\ 0 & 0 & \sqrt{2D_{\perp}} \end{bmatrix}, \quad (6)$$

Diffusion parallel to the wall is (Faxén, 1922):

$$\frac{D_{\parallel}}{D_{\infty}} = 1 - \frac{9}{16} \left(\frac{r}{d} \right) + \frac{1}{8} \left(\frac{r}{d} \right)^3 - \frac{45}{256} \left(\frac{r}{d} \right)^4 - \frac{1}{16} \left(\frac{r}{d} \right)^5, \quad (7)$$

where r (m) is the colloid radius and d (m) is the separation distance between the colloid surface and the wall. Diffusion normal to the wall is (Brenner, 1961):

$$\frac{D_{\perp}}{D_{\infty}} = \frac{6 \left(\frac{d}{r} \right)^2 + 10 \left(\frac{d}{r} \right) + 4}{6 \left(\frac{d}{r} \right)^2 - 3 \left(\frac{d}{r} \right) - 1}, \quad (8)$$

where the free diffusion coefficient is calculated from the Stokes–Einstein equation as (Einstein, 1906):

$$D_{\infty} = \frac{k_B T}{6\pi\mu r}, \quad (9)$$

where k_B (J K^{-1}) is the Boltzmann constant and T (K) is the absolute temperature of the fluid.

2.6. Derjaguin–Landau–Verwey–Overbeek (DLVO) Theory

DLVO theory describes the forces between charged surfaces interacting through a liquid medium (Chrysikopoulos and Syngouna, 2012). These forces also depend on the small separation distance between a colloid and the fracture wall, d . The total DLVO interaction energy is (Loveland et al., 1996):

$$\Phi_{\text{DLVO}} = \Phi_{\text{VDW}}(d) + \Phi_{\text{dl}}(d) + \Phi_{\text{Born}}(d), \quad (10)$$

where Φ_{VDW} (J), Φ_{dl} (J), and Φ_{Born} (J) are van der Waals, double-layer, and Born potential energies, respectively. Forces were calculated as the derivative of (10) with respect to the distance d of the secondary minimum potential.

The van der Waals interaction energy for sphere-plate interaction is (Gregory, 1981):

$$\Phi_{\text{VDW}}(d) = -\frac{A_{123}r}{6d} \left(1 + \frac{14d}{\lambda_w} \right)^{-1}, \quad (11)$$

where A_{123} (J) is the combined Hamaker constant and λ_w (m) is the

characteristic wavelength of sphere-plate interactions.

The double-layer interaction energy for sphere-plate interaction is (Hogg et al., 1966):

$$\Phi_{dl}(d) = \pi \epsilon_r \epsilon_0 r \left\{ 2\Psi_p \Psi_s \ln \left[\frac{1 + \exp(-\kappa d)}{1 - \exp(-\kappa d)} \right] + (\Psi_p^2 + \Psi_s^2) \ln [1 - \exp(-2\kappa d)] \right\}, \quad (12)$$

where $\epsilon_r = \epsilon/\epsilon_0$ (–) is the relative dielectric constant of the suspending liquid, ϵ ($C^2 J^{-1} m^{-1}$) is the dielectric constant of the suspending liquid, ϵ_0 ($C^2 J^{-1} m^{-1}$) is the permittivity of free space, Ψ_p and Ψ_s (V) the surface potentials of the colloid particle and the fracture surface (wall), respectively, and κ (m) the inverse diffusive layer thickness, or the Debye–Hückel parameter, which is:

$$\kappa = \sqrt{\frac{2I_s N_A 10^3 e^2}{\epsilon_r \epsilon_0 k_B T}}, \quad (13)$$

where I_s ($mol L^{-1}$) is the ionic strength, N_A (mol^{-1}) is Avogadro's number, and e (C) is the elementary charge.

The Born interaction energy for sphere-plate interaction is (Ruckenstein and Prieve, 1976):

$$\Phi_{Born}(d) = \frac{A_{123} \sigma_{Born}^6}{7, 560} \left[\frac{8r + d}{(2r + d)^7} + \frac{6r - d}{d^7} \right], \quad (14)$$

where σ_{Born} (m) is the Born collision parameter, commonly $\sigma_{Born} = 5\text{Å}$.

3. Colloid transport

Although the irregular shapes of natural colloids can certainly impact their transport and attachment characteristics, here they were represented as neutrally buoyant spheres to focus on how wall effects on diffusion and variable surface-attachment characteristics influenced colloid transport. A monodisperse plume of 1,000 colloids with 0.05- μm radii was released instantaneously into each realization of the fracture flow field at $x = 0$, where $\eta = 0.025$ m ($\eta = 0$ at $x = 4$ m) across the inlet using a flux-weighted scheme (Reimus, 1995), and colloid positions were tracked with time. The shape of the curve describing the DLVO potential (Fig. 3) has the secondary minimum separated from the

Table 1
DLVO parameters.

Parameter	Value	Reference
σ_{Born}	5×10^{-10} m	Ruckenstein and Prieve (1976) and Chrysikopoulos and Syngouna (2012)
A_{123}	7.5×10^{-21} J	Murray and Parks (1978)
λ_w	10^{-7} m	Gregory (1981)
ϵ_r	78.4	Weast (1984)
ϵ_0	8.854×10^{-12} C ² J ⁻¹ m ⁻¹	Weast (1984)
k_B	1.38066×10^{-23} J K ⁻¹	Weast (1984)
N_A	6.0221367×10^{23} mol ⁻¹	Weast (1984)
e	-1.60219×10^{-19} C	Weast (1984)
T	298 K	This study
I_s	5×10^{-4} mol L ⁻¹	This study
γ	19,600 N m ⁻³	This study
μ	8.9×10^{-4} Pa s	Kestin et al. (1978)
Ψ_p	-30 mV	Chrysikopoulos and Syngouna (2012)
Ψ_s	roughly -60 to -10 mV	Chrysikopoulos et al. (2012) and Syngouna and Chrysikopoulos (2013)

primary minimum by a maximum potential that cannot be overcome (for the parameters used in this study shown in Table 1). Because of this, when a colloid diffused closer to the wall than the location of the secondary minimum, it was assumed to attach in the secondary minimum. In subsequent time steps, the potential diffusive movement of each attached colloid was calculated. The advective force exerted on a colloid was (Goldman et al., 1967; O'Neill, 1968):

$$F = 1.7009(6\pi r \mu U_{loc}), \quad (15)$$

where the local velocity was:

$$U_{loc} = 6 \left(\frac{r}{b} \right) \left(1 - \frac{r}{b} \right) \sqrt{u_x^2(x, y) + u_y^2(x, y)}. \quad (16)$$

If this force exceeded the Φ_{DLVO} attachment force, then the colloid was released back into fracture flow at the location of the DLVO minimum plus one colloid-diameter distance toward the fracture center.

Two cases without attachment were run without (Case 1) and with (Case 2) wall effects on diffusion. Next, three cases of surface-potential correlation were developed for this investigation. Parameters in Table 1

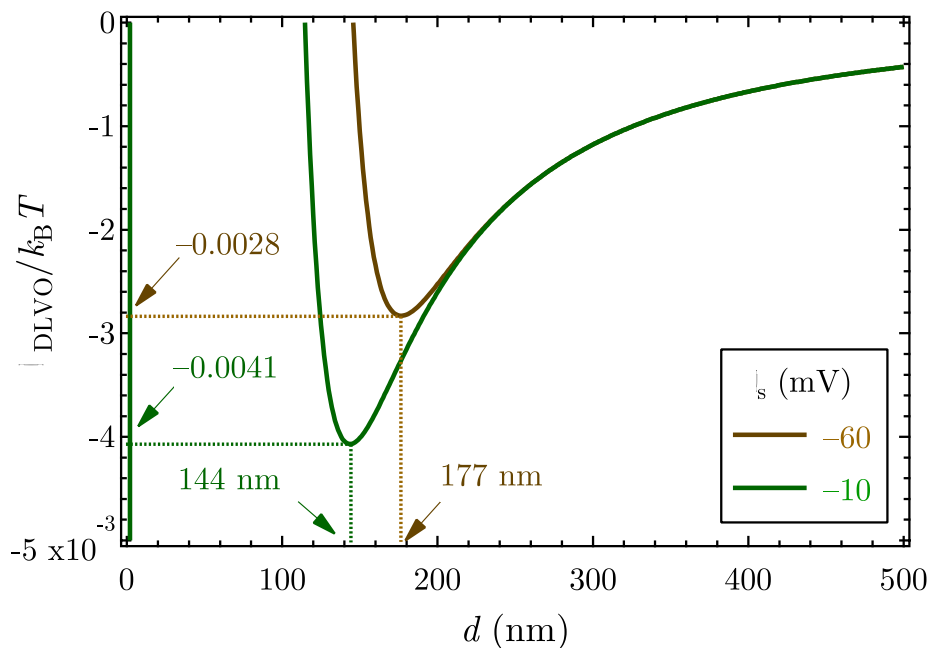


Fig. 3. DLVO potentials as a function of distance from the wall for the minimum and maximum Ψ_s used in these calculations showing the secondary minima.

are appropriate for neutrally buoyant colloids in water at room temperature. The ionic strength of the suspending liquid, which was a sensitive parameter, was selected to ensure that neither too few nor too many colloids attached in these simulations to represent a realistic system. In all cases, the normally distributed surface potentials were assigned a mean of -35 mV with a standard deviation of 5 mV (all surface potentials fell between -13.1 and -58.4 mV). These yielded a range of separation distances (locations of the minimum) from 144 to 177 nm. The first instance (Case 3) negatively correlated the surface potential with the local aperture. The second instance (Case 4) randomly assigned surface potentials. The third instance (Case 5) positively correlated the surface potentials to the local fracture aperture. As specified, surface-potential histograms for Cases 3 and 5 look similar, but the distributions were skewed oppositely so that high surface potentials for Case 3 corresponded to locations of low surface potential in Case 5. Such correlations could arise, for example, through sorption or precipitation of dissolved constituents along preferential flow paths. Another example, albeit for multi-phase systems, is altered surface wettability (e.g., invasion of supercritical CO_2), which is important because two-phase flow is strongly governed by the aperture field.

4. Results and discussion

Five scenarios were run with the model: Case 1 - no attachment and no wall effects on diffusion (i.e., $D_{\perp} = D_{\parallel} = D_{\infty}$), Case 2 - no attachment with wall effects on diffusion, and the three attachment scenarios with negative (Case 3), zero or random (Case 4), and positive (Case 5) correlation of the wall surface potential with the local fracture aperture. Cases 3 through 5 were run both with and without wall effects on diffusion, but the results were statistically equivalent so only simulations without wall effects are discussed. When both attachment and wall effects were included, sensitivity in the transport simulations was due to variability in attachment characteristics (wall potential correlated to local aperture); altered diffusivities due to wall proximity were clearly higher-order effects. An ensemble average was taken across the 100 fracture realizations to quantify uncertainty. Fig. 4 shows

Table 2
Summary of colloid-plume transport characteristics.

Case	Minimum	Median	Mean	Maximum	Standard deviation
Time to exit (hours)					
1	29.5	34.6	34.9	41.9	3.0
2	29.7	34.8	35.2	42.1	3.0
3 (-)	35.0	39.3	40.8	NA	6.2
4 (0)	35.1	39.9	41.1	NA	6.0
5 (+)	35.4	40.3	42.0	NA	6.5
Colloids exited (remainder attached)					
3 (-)	318	846	817	968	116
4 (0)	114	639	592	887	173
5 (+)	47	457	432	808	181

snapshots of suspended (left) and attached (right) colloids at 10 (top), 20 (middle), and 30 h (bottom) for Case 4.

Without attachment, all colloids successfully negotiated the fractures so exit times were compared. As shown in Table 2, there were only slight differences in exit times between Cases 1 and 2. With the diffusive wall effects considered, the average colloid exit time increased from 34.9 to 35.2 h. With a fairly large average aperture, wall effects on diffusion were only evident when colloids were within about one colloid diameter from the wall, which was only about 0.5% of the average aperture. For smaller average apertures, wall effects on diffusion would be more prominent. Because wall effects on diffusion were minimally important for the fractures studied here; they were not presented for subsequent cases.

Fig. 5 shows the time evolution for the first and second moments for suspended and attached colloids for Cases 3–5. The slightly sublinear slopes of the first moments for all Cases indicated a fairly constant velocity that decreased only slightly over time as colloids attached. There was a trend of delayed transit time of particles (evident in the time statistics in Table 2 across all realizations) when the surface potential was correlated negatively, randomly, and positively with the local fracture aperture (see Table 2). The opposite trend held for the

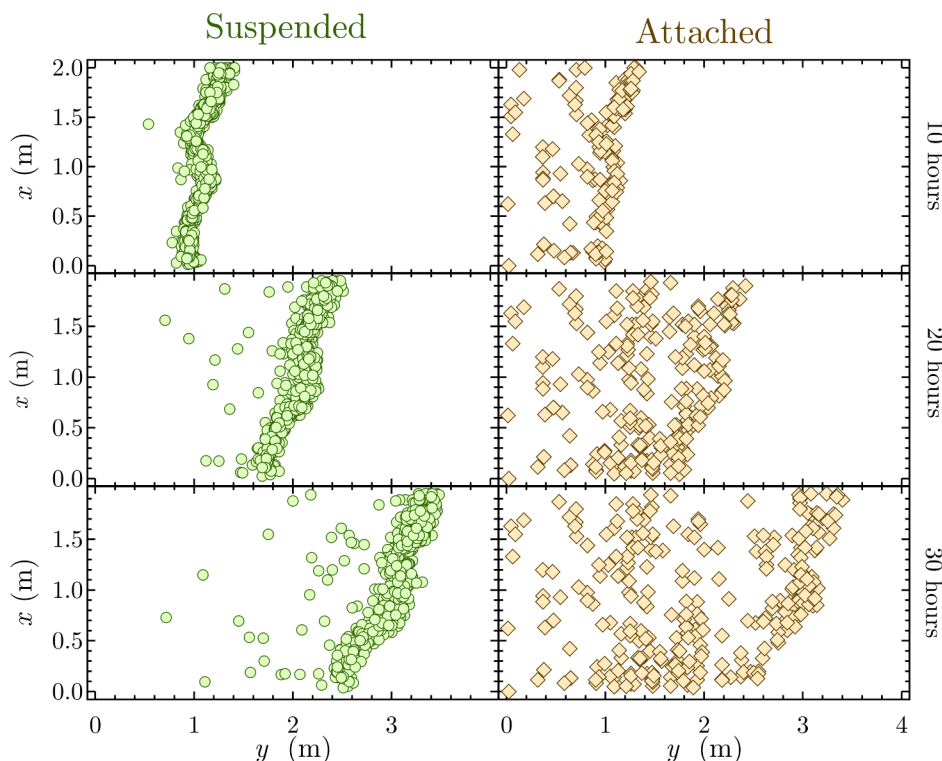


Fig. 4. Snapshots of suspended (left) and attached (right) colloids at 10 (top), 20 (middle), and 30 h (bottom) for Case 4.

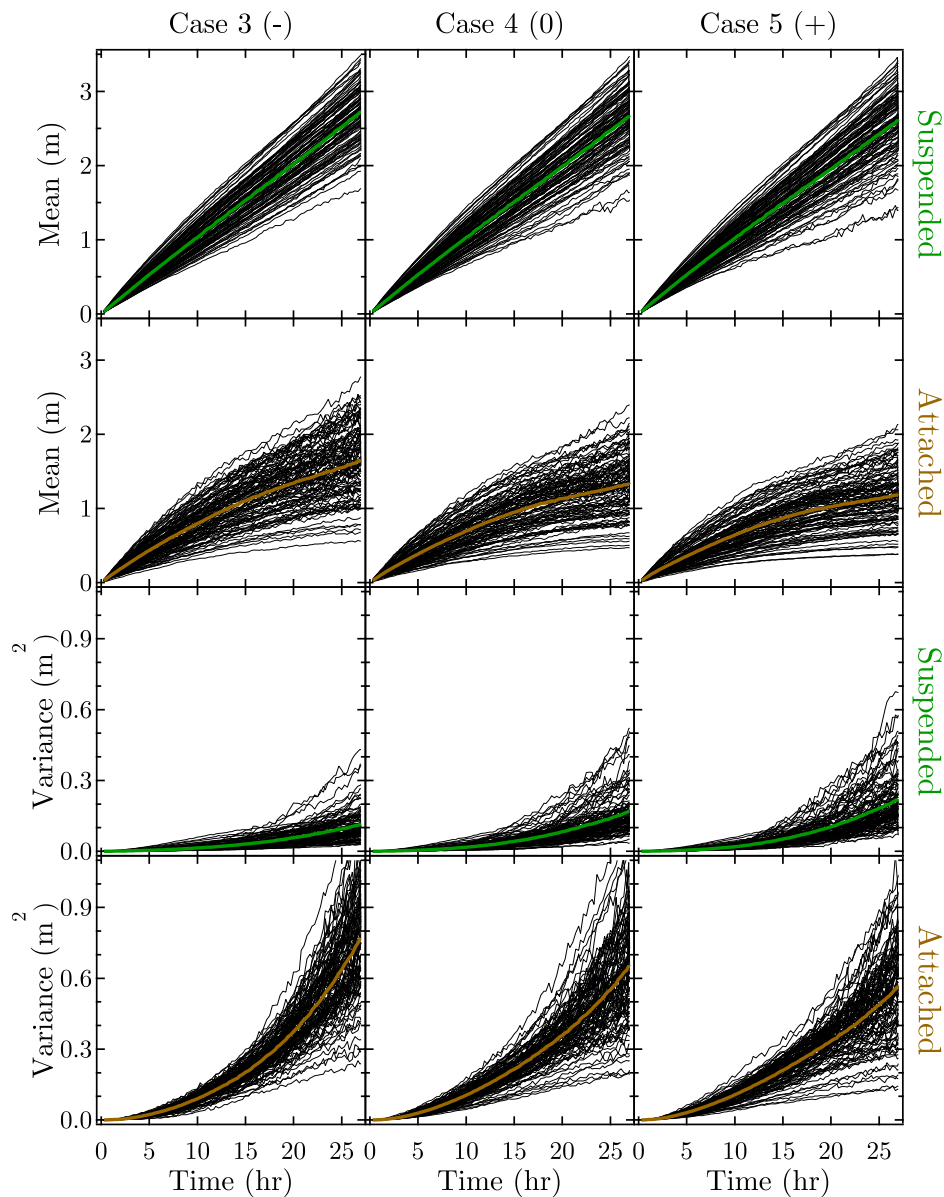


Fig. 5. First and second moments for suspended and attached colloids for Cases 3 through 5.

total number of colloids exiting the fracture. Although the standard deviations were sufficiently high that the trend was statistically significant only to $p < 0.08$ for increasing mean exit times, for the trend of decreasing number of colloids exiting from Cases 3 to 5, $p < 0.001$. These results were consistent with colloids following preferential flow paths through larger apertures with less attachment when surface potential was negatively correlated with local aperture (Case 3). Because of this, colloids flowing through preferential flow paths of larger apertures experienced less attachment (more colloids exiting) and exited slightly earlier on average. Also, because the force exerted on a colloid according to (15) is a function of local velocity (16), detachment was more likely in regions with larger apertures.

Given the difficulty in drawing conclusions from Fig. 5, two additional analyses were conducted. Fig. 6 shows violin plots of the first and second spatial moments (Chrysikopoulos et al., 1990; Katzourakis and Chrysikopoulos, 2018) for both the suspended and attached colloids calculated at the instant when the first colloid exited the fracture. Ranges, frequencies, means, and medians for the 100 realizations are indicated. For Case 3, colloids preferentially transported through the fracture because they tended to enter high-flow, large-aperture regions

where they underwent less attachment (have the largest first moment). Variances (second moment) increased for suspended colloids when comparing Cases 3 to 4 to 5 because spreading increased when more members of the colloid plume (temporarily) attached to the fracture surface. For attached colloids, both first and second moments decreased from negatively (Case 3), to zero (Case 4), to positively (Case 5) correlated surface potentials to apertures, consistent with more colloids attaching along the larger aperture, preferential flow paths.

Finally, tailing was investigated by calculating power-law fits to the tails of log-transformed breakthrough curves (i.e., residence time distributions or RTDs) (Wang and Cardenas, 2017). RTDs can be approximated using the definition of a breakthrough curve:

$$C(t) = \frac{N(t)}{N_0}, \tag{17}$$

which can be used to characterize the relationship between $dC(t)/dt$ and t and thus provide an additional metric for examining non-Fickian transport features like heavy tailing. Fig. 7 shows example rates of change of cumulative particles, $dC(t)/dt$, as a function of time (i.e., RTD in log-log space) for Cases 3 to 5. Each red line is the power-law fit to

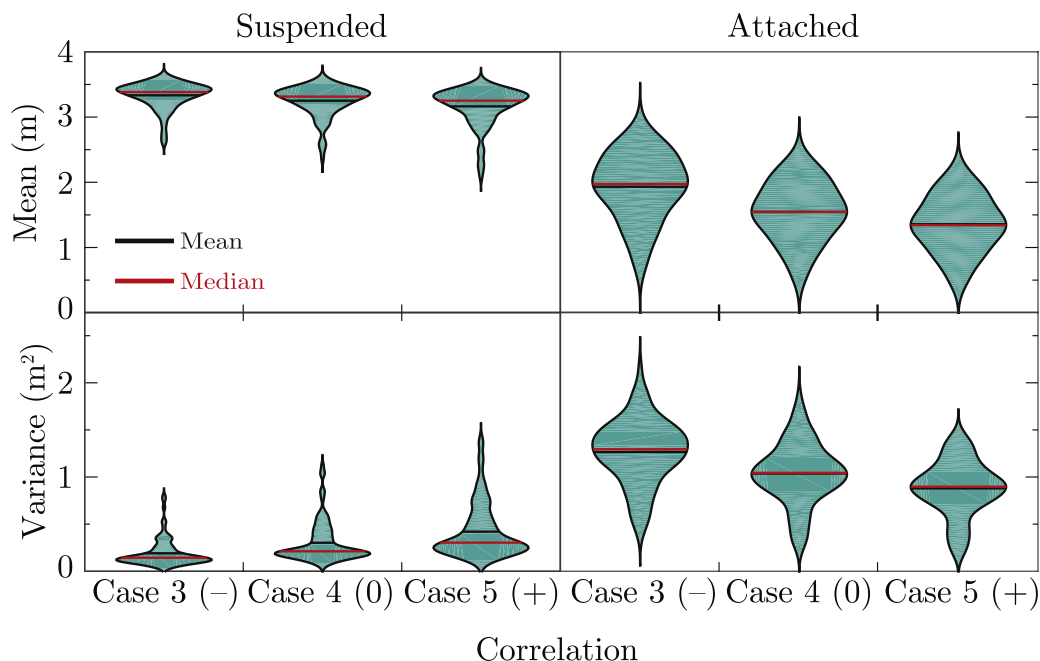


Fig. 6. Violin plots for Cases 3 through 5. A violin plot is similar to, but more informative than, a box-and-whisker plot because the full distributions of data are shown.

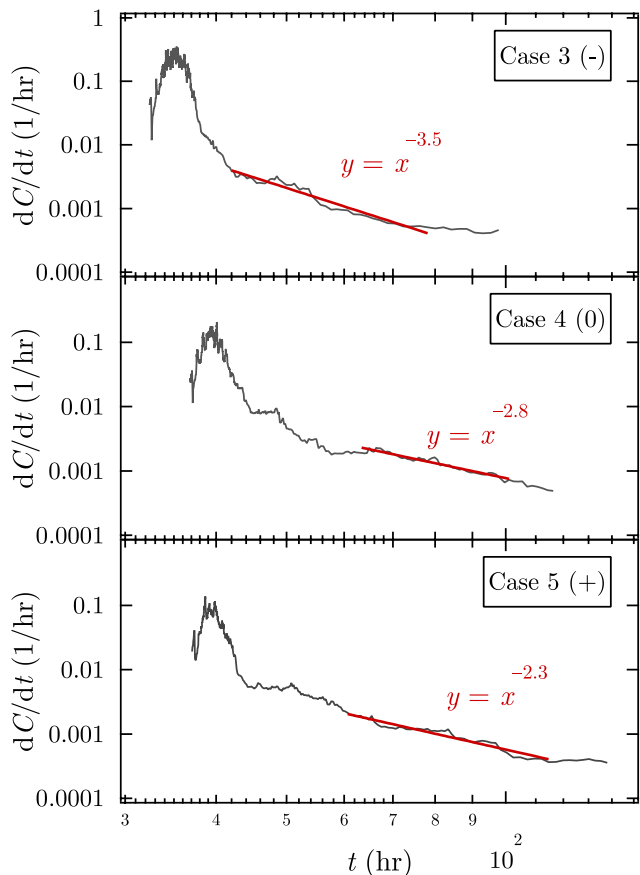


Fig. 7. Example RTD log-log plots of rate of change of colloid concentration with time for Cases 3 to 5. The red lines were fit to the tails of the breakthrough curves (70 of the last 80 data points, but not the last 10) and their slopes are the power-law exponents, n .

Table 3

Statistical summary of power-law exponents, n .

Case	Minimum	Median	Mean	Maximum	Standard deviation
1	14.9	9.0	9.1	2.3	4.2
2	10.9	8.4	7.2	1.4	3.8
3(-)	9.6	2.9	4.0	0.3	3.0
4(0)	7.8	2.2	2.4	0.0	1.4
5(+)	6.4	1.9	2.1	0.0	1.4

70 of the last 80 data points (the final 10 were discarded). The power-law exponent, n , is the slope of the red line. Statistical measures for n across the 100 fractures are listed in Table 3. Larger n indicates less tailing and vice versa. The largest n s were for Cases 1 and 2 without attachment. For Case 3, n was larger than the next two cases meaning it took less time for these colloids to exit the fracture. For Cases 4 and 5, n was smaller indicating that some colloids took a long time to exit; $n < -3$ suggests an infinitely long time for colloids to exit the fracture indicating the potential for effectively permanent attachment.

This analysis has identified that wall effects on diffusion are a secondary consideration when colloid attachment is important, but additional discussion of relevance and limitations is warranted. Because colloid diffusion is only altered by wall proximity when they are less than a few diameters away, effects in fractures with apertures several thousand times larger than the colloids were minimal. If apertures were on the order of colloid size; however, both attachment and physical straining become important processes to consider. Regarding the demonstrated importance of surface-potential variability, it is acknowledged that the most common situation would not be one where it was correlated to aperture (although for reactive or multi-phase flows this is possible). Nevertheless, this research highlights the importance of better characterizing variability in wall surface potentials because of their effects on colloid transport.

5. Conclusions

A particle-tracking simulation of colloids flowing through variable-aperture fractures subject to wall effects on diffusion as well as colloid

attachment according to DLVO energies was developed. The 100 synthetic, variable-aperture-fracture realizations were generated with the code SPRT2D parameterized by the statistical properties of a real, rough fracture. It was determined that when wall effects on diffusion were included, colloids took slightly longer to exit the fractures because of decreased diffusion near the walls, but for the fractures with a fairly large average aperture studied here, this change was minimal. When the fracture-wall surface potential was correlated either negatively, randomly, or positively with the local aperture, colloid transport was altered. Because colloids preferentially travel in large-aperture regions of the fracture, when wall surface potential was negatively correlated with local aperture, fewer colloids attached, and those colloids that did so exited sooner than when fracture-wall surface potential was not correlated or positively correlated with the local aperture. Power-law fits to the tails of the breakthrough curves confirmed that tailing was more pronounced when colloids were subject to attachment. Increased tailing (up to infinite residence time) was observed as the surface potential became neutrally and then positively correlated with the local fracture aperture. For the fractures studied here, this research highlights the importance of variability in surface-attachment characteristics (wall potential) on colloid transport while wall effects on diffusion were higher-order processes.

References

- Abdel-Salam, A., Chrysikopoulos, C.V., 1995. Modeling of colloid and colloid-facilitated contaminant transport in a 2-dimensional fracture with spatially variable aperture. *Transp. Porous Media* 20, 197–221.
- Ahlstrom, S., Foote, H., Arnett, R., Cole, C., Serne, R., 1977. Multicomponent Mass Transport Model: Theory and Numerical Implementation (Discrete-parcel-random-walk Version), Report BNWL-1717. Battelle Pacific Northwest Labs, Richland, WA (USA).
- Bales, R.C., Gerba, C.P., Grondin, G.H., Jensen, S.L., 1989. Bacteriophage transport in sandy soil and fractured tuff. *Appl. Environ. Microbiol.* 55, 2061–2067.
- Berkowitz, B., 2002. Characterizing flow and transport in fractured geological media: A review. *Adv. Water Resour.* 25, 861–884.
- Bossart, P., Hermanson, J., Mazurek, M., 2001. Äspö Hard Rock Laboratory, Analysis of Fracture Networks Based on the Integration of Structural and Hydrogeological Observations on Different Scales, Report TR-01-21. Svensk Kärnbränslehantering AB.
- Brenner, H., 1961. The slow motion of a sphere through a viscous fluid towards a plane surface. *Chem. Eng. Sci.* 16, 242–251.
- Cardenas, M.B., Slottke, D.T., Ketcham, R.A., Sharp Jr., J.M., 2007. Navier-stokes flow and transport simulations using real fractures shows heavy tailing due to eddies. *Geophys. Res. Lett.* 34, L14404.
- Chrysikopoulos, C.V., Syngouna, V.I., 2012. Attachment of bacteriophages MS2 and Φ X174 onto kaolinite and montmorillonite: Extended-DLVO interactions. *Colloids Surf., B* 92, 74–83.
- Chrysikopoulos, C.V., Kitanidis, P.K., Roberts, P.V., 1990. Analysis of one-dimensional solute transport through porous media with spatially variable retardation factor. *Water Resour. Res.* 26, 437–446.
- Chrysikopoulos, C.V., Syngouna, V.I., Vasiliadou, I.A., Katzourakis, V.E., 2012. Transport of *Pseudomonas putida* in a 3-D bench scale experimental aquifer. *Transp. Porous Media* 94, 617–642.
- Delay, F., Ackerer, P., Danquigny, C., 2005. Simulating solute transport in porous or fractured formations using random walk particle tracking. *Vadose Zone J.* 4, 360–379.
- Drever, I., 1985. The Chemistry of Weathering, volume 149 of *Series C: Mathematical and Physical Sciences*. D. Reidel Publishing Company, Dordrecht, Holland.
- Einstein, A., 1906. A new determination of molecular dimensions. *Ann. Phys.* 19, 289–306.
- Elimelech, M., Gregory, J., Jia, X., Williams, R.A., 1995. Particle Deposition & Aggregation. Butterworth-Heinemann, Woburn.
- Faxén, H., 1922. Der widerstand gegen die bewegung einer starren kugel in einer zahren flüssigkeit, die zwischen zwei parallelen ebenen wänden eingeschlossen ist. *Ann. Phys.* 373, 89–119.
- Goldman, A., Cox, R., Brenner, H., 1967. Slow viscous motion of a sphere parallel to a plane wall - II Couette flow. *Chem. Eng. Sci.* 22, 653–660.
- Gregory, J., 1981. Approximate expressions for retarded van der waals interaction. *J. Colloid Interface Sci.* 83, 138–145.
- Gutjahr, A.L., 1989. Fast Fourier Transforms for Random Field Generation: Project Report for Los Alamos Grant to New Mexico Tech, Thesis. New Mexico Institute of Mining and Technology.
- Hogg, R., Healy, T.W., Fuerstenau, D., 1966. Mutual coagulation of colloidal dispersions. *Trans. Faraday Soc.* 62, 1638–1651.
- James, S.C., Chrysikopoulos, C.V., 1999. Transport of polydisperse colloid suspensions in a single fracture. *Water Resour. Res.* 35, 707–718.
- James, S.C., Chrysikopoulos, C.V., 2000. Transport of polydisperse colloids in a saturated fracture with spatially variable aperture. *Water Resour. Res.* 36, 1457–1465.
- James, S.C., Chrysikopoulos, C.V., 2004. Dense colloid transport in a bifurcating fracture. *J. Colloid Interface Sci.* 270, 250–254.
- James, S.C., Chrysikopoulos, C.V., 2011. Monodisperse and polydisperse colloid transport in water-saturated fractures with various orientations: Gravity effects. *Adv. Water Resour.* 34, 1249–1255.
- James, S.C., Bilezikjian, T.K., Chrysikopoulos, C.V., 2005. Contaminant transport in a fracture with spatially variable aperture in the presence of monodisperse and polydisperse colloids. *Stoch. Env. Res. Risk Assess.* 19, 266–279.
- Katzourakis, V.E., Chrysikopoulos, C.V., 2018. Impact of spatially variable collision efficiency on the transport of biocolloids in geochemically heterogeneous porous media. *Water Resour. Res.* 54.
- Kestin, J., Sokolov, M., Wakeham, W.A., 1978. Viscosity of liquid water in the range 8 °C to 150 °C. *J. Phys. Chem. Ref. Data* 7, 941–948.
- Kickmaier, W., Alexander, W.R., Vomvoris, S., McKinley, I.G., 2000. Grimsel 2000 – Status of international projects at the grimsel test site (GTS). In: Hart, K.P., Lumpkin, R., Gregory (Eds.), *Materials Research Society Symposium*, vol. 663, pp. 893–900. August 27–31.
- Kinzelbach, W., 1988. The random walk method in pollutant transport simulation. In: *Groundwater Flow and Quality Modelling*. Springer, pp. 227–245.
- Kitanidis, P.K., 1994. Particle-tracking equations for the solution of the advection-dispersion equation with variable coefficients. *Water Resour. Res.* 30, 3225–3227.
- Loveland, J.P., Ryan, J.N., Amy, G.L., Harvey, R.W., 1996. The reversibility of virus attachment to mineral surfaces. *Colloids Surf., A* 107, 205–221.
- McKenna, S.A., James, S.C., 2007. Modelling Task 6B2 (Äspö Modelling), Report SAND2007-6363. Sandia National Laboratories.
- Minasny, B., McBratne, A.B., Whelan, B.M., 1999. VESPER – Program for automatic Variogram Estimation and Spatial Prediction with ERror. *Pedometrics* 99, 66.
- Murray, J.P., Parks, G.A., 1978. Particulates in Water: Characterization, Fate, Effects, and Removal. American Chemical Society.
- NRC, 1999. Disposal of High-Level Radioactive Wastes in a Proposed Geological Repository at Yucca Mountain, 10 CFR 63, Report, Code of Federal Regulations, Title 10, Part 63. U.S. Nuclear Regulatory Commission.
- NUMO, 2004. Evaluating Site Suitability for a HLW Repository, Scientific Background and Practical Application of NUMO's Siting Factors, Report NUMO-TR-04-04. Nuclear Waste Management Organization of Japan.
- O'Neill, M.E., 1968. A sphere in contact with a plane wall in a slow linear shear flow. *Chem. Eng. Sci.* 23, 1293–1298.
- Ouyang, Y., Shinde, D., Mansell, R., Harris, W., 1996. Colloid-enhanced transport of chemicals in subsurface environments: A review. *Crit. Rev. Environ. Sci. Technol.* 26, 189–204.
- Reimus, P.W., 1995. The Use of Synthetic Colloids in Tracer Transport Experiments in Saturated Rock Fractures, Report LA-13004-T. Los Alamos National Laboratory.
- Reimus, P.W., James, S.C., 2002. Determining the random time step in a constant spatial step particle tracking algorithm. *Chem. Eng. Sci.* 57, 4429–4434.
- Ruckenstein, E., Prieve, D.C., 1976. Adsorption and desorption of particles and their chromatographic separation. *AIChE J.* 22, 276–283.
- Smith, L., Schwartz, F.W., 1980. Mass transport: 1. A stochastic analysis of macroscopic dispersion. *Water Resour. Res.* 16, 303–313.
- Stoll, M., Huber, F., Schill, E., Schäfer, T., 2017. Parallel-plate fracture transport experiments of nanoparticulate illite in the ultra-trace concentration range investigated by laser-induced breakdown detection (LIBD). *Colloids Surf., A* 529, 222–230.
- Syngouna, V.I., Chrysikopoulos, C.V., 2013. Cotransport of clay colloids and viruses in water saturated porous media. *Colloids Surf., A* 416, 56–65.
- Tompson, A.F.B., Gelhar, L.W., 1990. Numerical simulation of solute transport in three-dimensional, randomly heterogeneous porous media. *Water Resour. Res.* 26, 2541–2562.
- Wang, L., Cardenas, M.B., 2014. Non-fickian transport through two-dimensional rough fractures: Assessment and prediction. *Water Resour. Res.* 50, 871–884.
- Wang, L., Cardenas, M.B., 2015. An efficient quasi-3d particle tracking-based approach for transport through fractures with application to dynamic dispersion calculation. *J. Contam. Hydrol.* 179, 47–54.
- Wang, L., Cardenas, M.B., 2017. Transition from non-Fickian to Fickian longitudinal transport through 3-D rough fractures: Scale-(in) sensitivity and roughness dependence. *J. Contam. Hydrol.* 198, 1–10.
- Wang, L., Cardenas, M.B., Slottke, D.T., Ketcham, R.A., Sharp Jr., J.M., 2015. Modification of the local cubic law of fracture flow for weak inertia, tortuosity and roughness. *Water Resour. Res.* 51, 2064–2080.
- Weast, R.C. (Ed.), 1984. *Handbook of Chemistry and Physics*, 64th ed. CRC Press.
- Zhang, W., Tang, X., Weisbrod, N., Guan, Z., 2012. A review of colloid transport in fractured rocks. *J. Mount. Sci.* 9, 770–787.